



3D Crust and Uppermost Mantle Structure beneath Tian Shan Region from ambient noise and earthquake surface waves

Xiao Xiao¹ (xiaox17@mail.ustc.edu.cn), Lianxing Wen^{2,1}

AGU 2017

S51D-0626

1. Laboratory of Seismology and Physics of Earth's Interior, University of Science and Technology of China

2. Department of Geosciences, State University of New York at Stony Brook

1. INTRODUCTION

As a typical active intracontinental mountain range in Central Asia, Tian Shan Mt serves as the prototype in studying geodynamic processes and mechanism of intracontinental mountain building. In Tian Shan Mt. and nearby area, There are three mainly geological blocks, Tarim basin, Tian Shan Mountain and Junggar basin. To figure out underground structure and geological evolution history there, We study 3D crust and the uppermost mantle structure beneath Tian Shan and close region using ambient noise and earthquake surface waves.

2. DATA AND METHODS

My data set contains 60 broad-band seismic stations mainly locating at foot of Tian Shan mountain and joint area (Fig. 1.). Several stations, situating at the southern foot of Altai Mt. and northern foot of Kunlun Mt., provide critical ray path coverage of Junggar and Tarim basins. Our dataset includes vertical component continuous record from 2015 to 2016 and teleseismic waveforms, whose magnitudes are over 5.5, focal depths are shallower than 200 km and happened during 2013 and 2016.

We combine the group velocity dispersion curves measured from ambient noise and earthquake surface waves, obtain lateral isotropic group velocity maps at different periods based on tomography and invert a 3D Vs model of crust and uppermost mantle down to about 70 km using a Monte Carlo Inversion method.

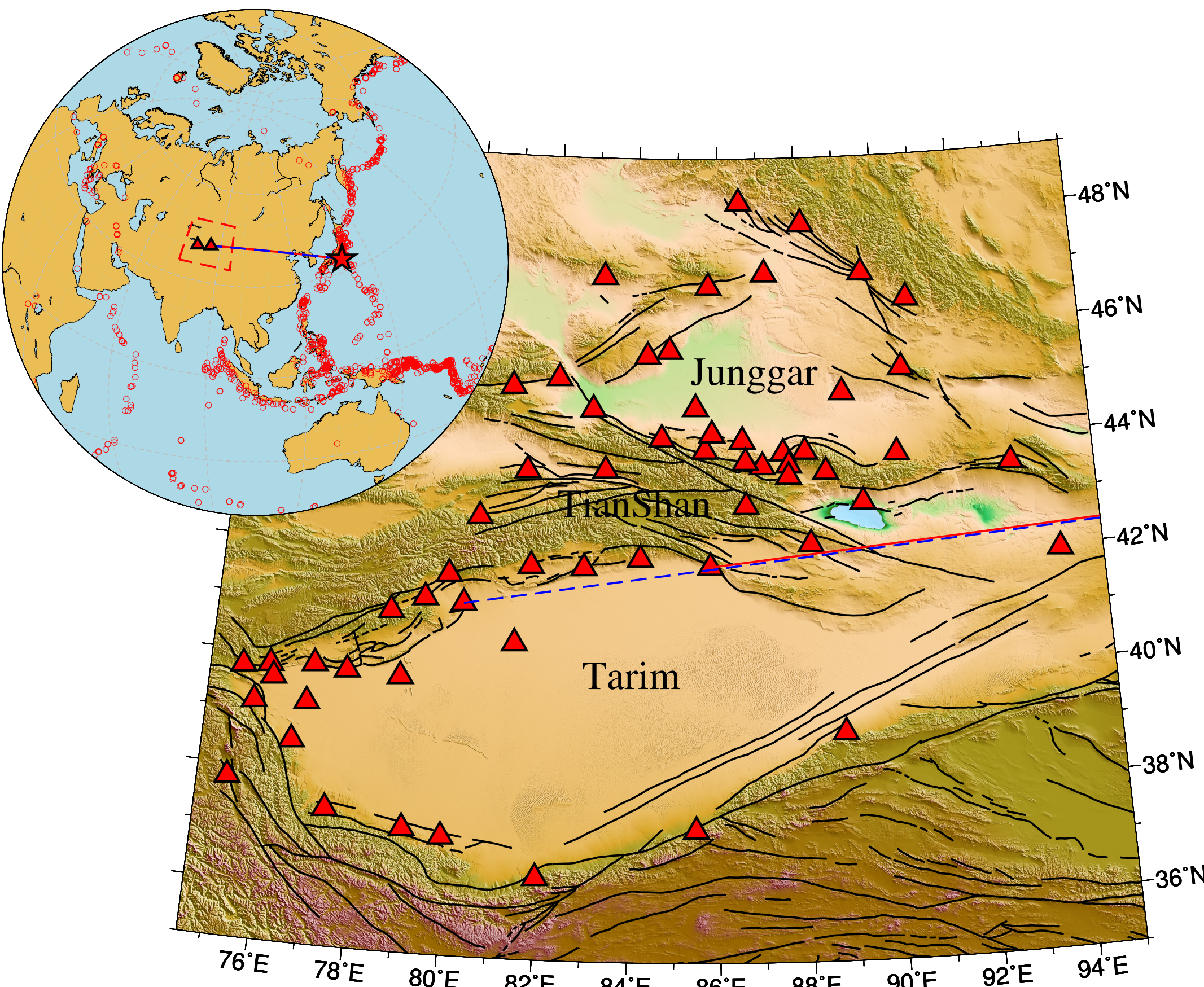


Fig. 1. Map of research area. Red triangles represent broad-band seismic stations in Tianshan area used in this study. Solid black thick lines show the faults. The insert (top left) depicts teleseismic distribution. Red circles represent epicenter of teleseismic used in this study, which happened from 2013 to 2016. Dashed red square is study area. Two triangles represent two stations named as AKS and KOL, which are in common line with this star-labelled earthquake.

We control quality of dispersion curves with spectral signal-noise-ratio (SNR) and standard deviation of measurements. For EGFs, we define signal-noise-ratio (SNR) as ratio of peak in signal window of surface wave and root mean standard (rms) in noise window at each period and we measure dispersion curves every trimesters which provides standard deviation of dispersion curve between a pair of station. We measure dispersion curves from teleseismic waveforms of different events of two stations. These curves give final dispersion curve to be median of them and standard deviation at each periods (Fig. 2.).

We take weighted average of reliable dispersion curves measured from EGF and teleseismic waveform to be final usable dispersion curves (Fig. 3.) and the weight is inverse of their standard deviation.

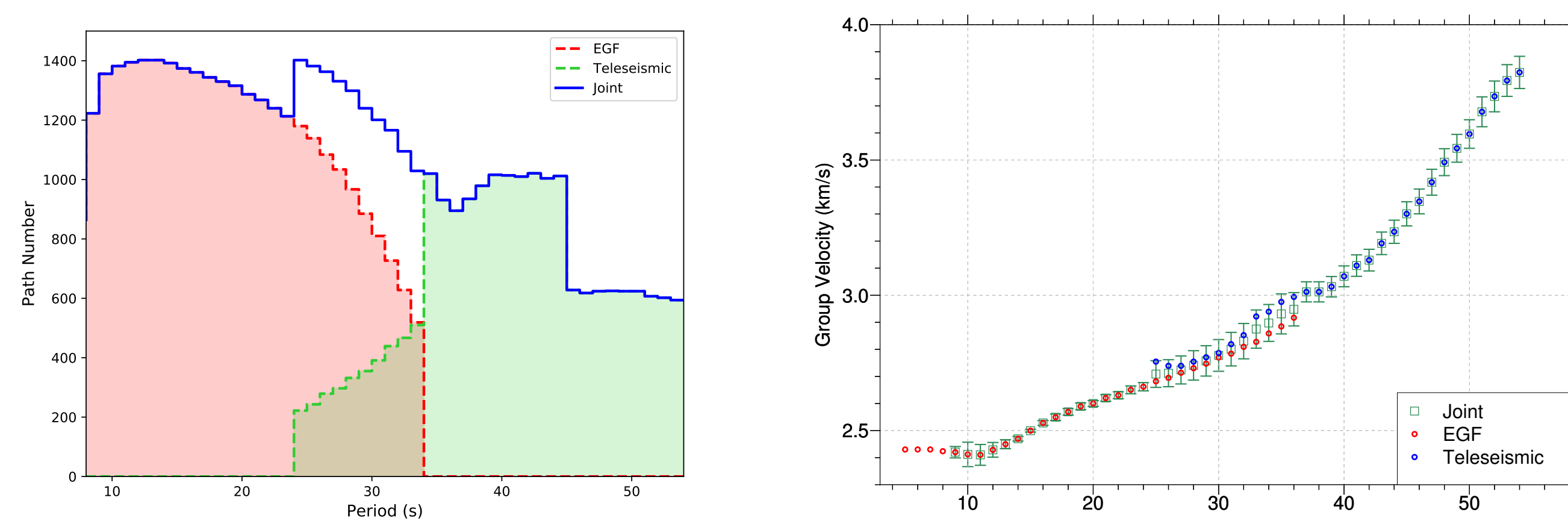


Fig. 2. Demos of combination of group velocity dispersion curves between two stations, AKS and KOL. Red circles denote dispersion points measured from EGF while blue circles represent those measured from teleseismic. Limegreen squares give combined dispersion curve. At overlap periods, green squares are weight average of blue and red circles, in which weights are inverse of their error which summation of their errors gives error of combined dispersion curve.

3. 2D GROUP VELOCITY MAPS

With combined dispersion curves, we use traditional surface wave tomography method to image 2D Rayleigh group velocity maps. Resolutions shown by fitted radius is consistent with that shown by checkerboard test, indicating this inversion can resolve $2^\circ \times 2^\circ$ anomalies (Fig. 3.).

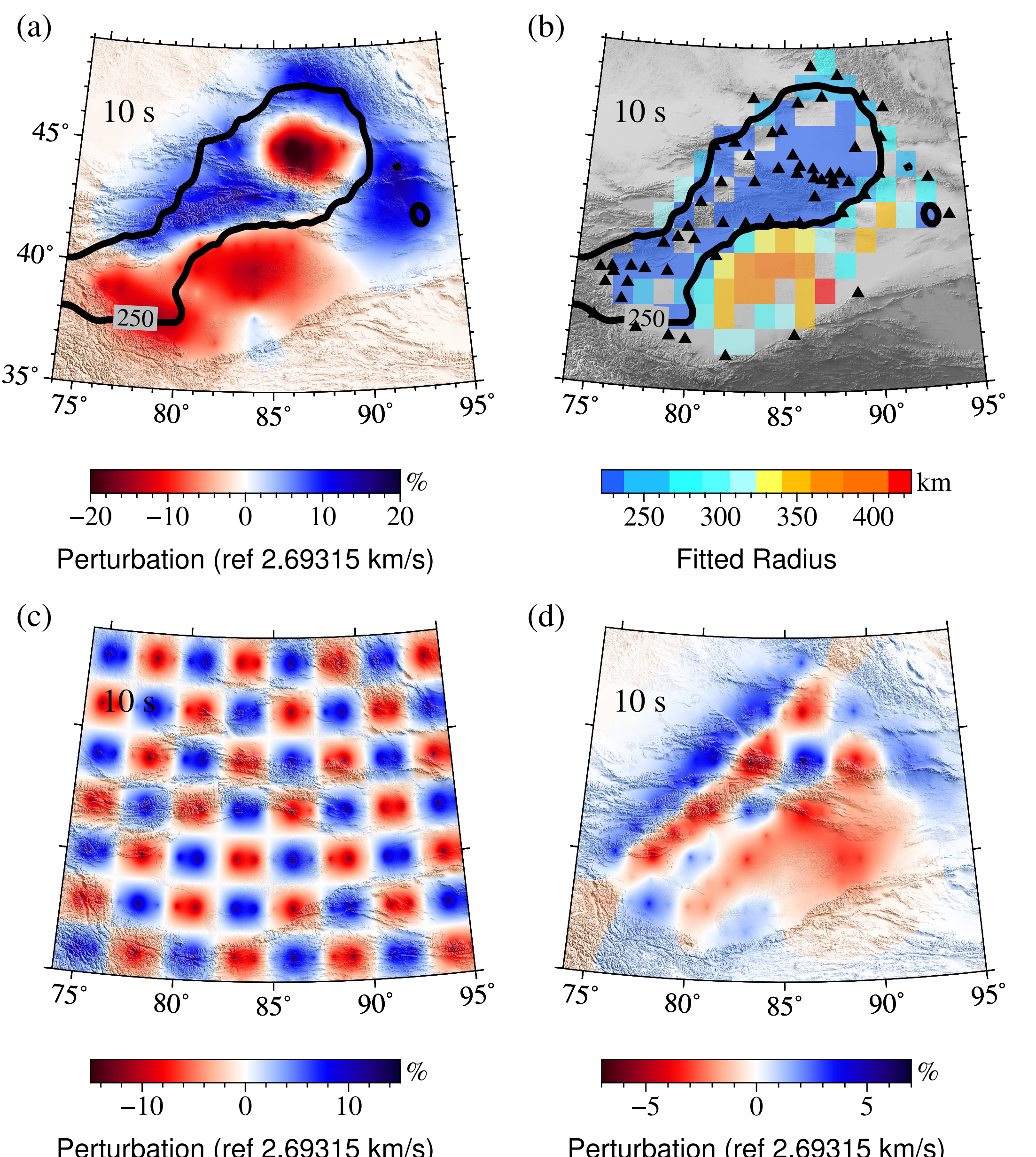


Fig. 3. Rayleigh group velocity tomography at 10 s. (a) 2D group velocity perturbation map refers to 2.69315 km/s, average group velocity of this area and the colorbar indicates percent. Solid black line encloses area with resolution better than 250 km/s. (b) Fitted radius distribution from resolution matrix. Black triangles indicate locations of seismic stations. Synthetic model (c) for checkerboard test and its recovered one (d). These models have similar symbols with panel (a).

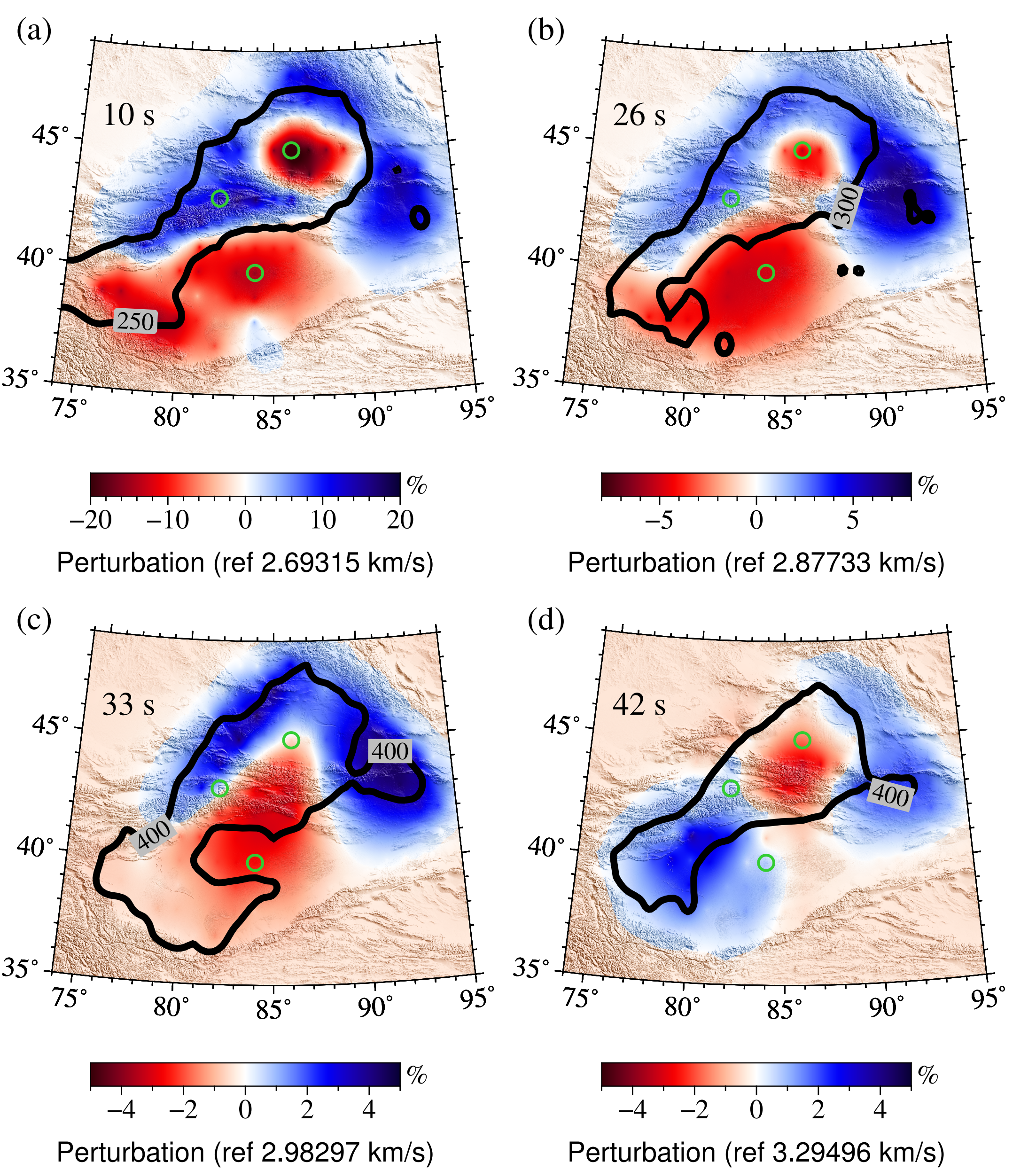


Fig. 4. Rayleigh group velocity perturbation relative to the median velocity at periods 10, 26, 33 and 42 s. The solid black line enclosed main area with resolution than labeled value. Three circles represent representative points to represent Tarim basin, Tian Shan Mt. and Junggar basin, separately, at which 1D shear velocity models are inverted in later section.

4. SHEAR WAVE VELOCITY MODELS

Surface wave tomography result provides Rayleigh group velocity dispersion curves at any points to do Monte Carlo Markov Chain inversion for three typical geological part.

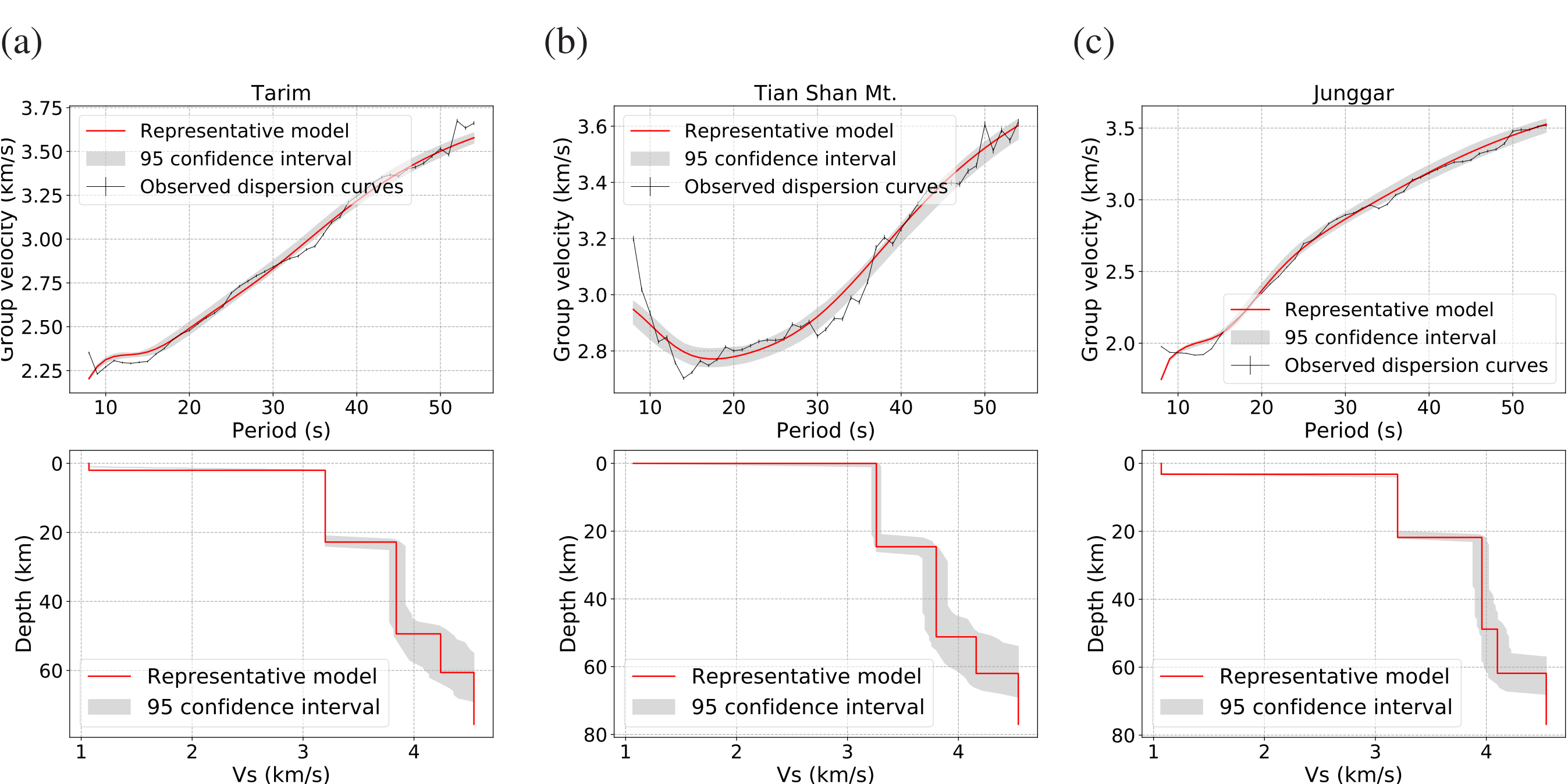


Fig. 5. Inverted models at three representative points, located at Tarim basin, Tian Shan Mountain and Junggar basin, separately. Observed dispersion curves (solid black lines with error bars) are extracted from 2D rayleigh group velocity maps. Shaded areas show the 95 percent confidence interval of the shear velocity model (below) and theoretical group velocity dispersion curve (upper). Red lines represent representative shear velocity model (below) and its synthetic dispersion curve (upper), which is closest to the average of all sampled models.

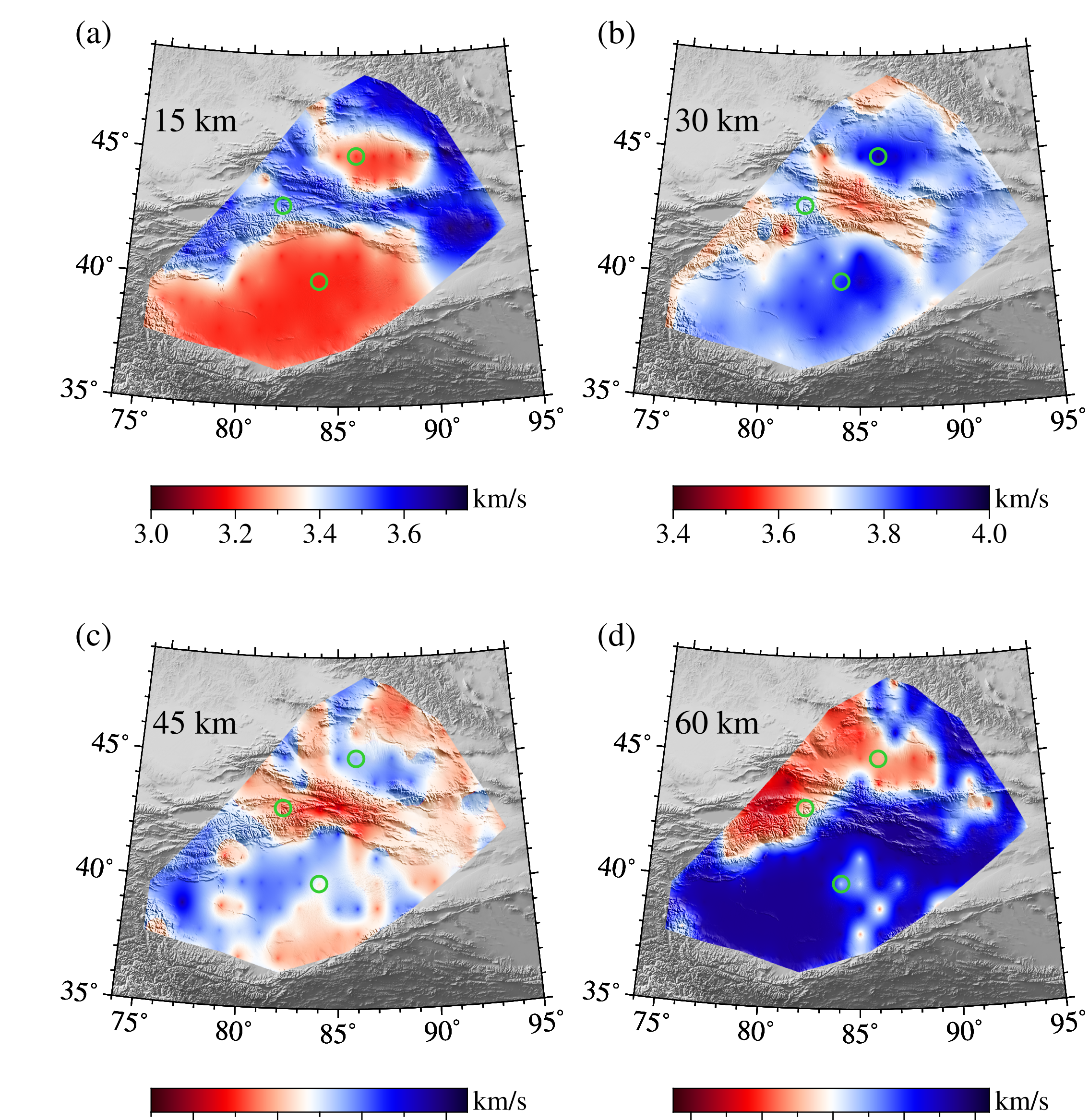


Fig. 6. Shear wave velocity maps at depths 15, 30, 45 and 60 km. Colored area indicates where there is path coverage. The green circles show locations of typical 1D shear wave velocity.

5. CONCLUSIONS

We collect a large dataset of high-quality PKiKP waveforms, and use PKiKP-PcP differential travel time residuals, PKiKP/PcP amplitude ratios, and PKiKP-PcP waveform differences to constrain ICB properties. Based on the observations, the ICB beneath Bearing Sea has a sharp and flat boundary, and the ICB beneath Mexico may have a bumpy ICB with a topographic height change of 5 km. PKiKP/PcP amplitude ratios are much larger than predictions, implying possible other factors which affects the amplitude ratios.